

CHARGED HIGGS PAIRS AT THE LHC: A NLO ANALYSIS

M. AHMED¹, L. BIERMANN¹, H. ITA^{1,2}, I. RUSetski^{1,3}, M. SPIRA¹ AND Y. YEDELKINA¹

¹ *PSI Center for Neutron and Muon Sciences, CH-5232 Villigen PSI, Switzerland*

² *Department of Astrophysics, University of Zurich, Winterthurerstrasse 190, 8057 Zurich, Switzerland*

³ *Albert Einstein Center for Fundamental Physics, Institute for Theoretical Physics, University of Bern, Sidlerstrasse 5, 3012 Bern, Switzerland*

Abstract

Charged Higgs-boson pair production at hadron colliders yields information about the trilinear couplings involving charged Higgs fields in extensions of the Standard Model (SM). We consider the type-I two-Higgs doublet model (2HDM) extension and obtain next-to-leading order QCD predictions for the charged-Higgs pair production (H^+H^- production). All production modes, i.e. Drell-Yan-like production, gluon fusion and vector-boson fusion are included in the analysis. We determine uncertainties originating from the scale dependence, the parton-density functions and strong coupling α_s at the LHC. We observe that the QCD corrections lead to a significant reduction of the relative scale dependences. These improved predictions will allow for a quantitative interpretation of experimental measurements, in case that charged Higgs states will be observed.

1 Introduction

With the discovery of a scalar resonance at the LHC [1] which is compatible with the Standard Model (SM) Higgs boson [2, 3] the theory of weak interactions is complete and renormalizable. However, since the SM does not explain several observations such as Dark Matter and Dark Energy as well as the matter-antimatter asymmetry of the Universe, it is considered incomplete and extensions beyond the SM (BSM) are expected. The search for BSM physics is concerned with two directions, *(i)* the search for deviations of the properties of SM particles from the SM prediction and *(ii)* the search for new particles. Since most of the known particle properties have been tested down to the per-cent or per-mille level, it is natural to focus BSM analyses on the properties of the discovered scalar resonance with a mass of about 125 GeV. Its properties are confirmed to agree with the SM Higgs boson at the 5–10% level which leaves ample room for potential deviations from the SM. Alternatively, searches for SM extensions including extended Higgs, gauge-boson and fermion sectors are actively pursued at the high-energy collider experiments at the LHC. In this work, we concentrate on extensions of the Higgs sector and

we will focus entirely on the production modes of charged Higgs states that arise naturally in extended Higgs sectors. As a particular example, we focus on the Two-Higgs Doublet Model (2HDM) of type I [5, 6].

This work adds to the presently available results for Drell–Yan-like production $q\bar{q} \rightarrow H^+H^-$ at next-to-leading order (NLO) [7]¹ and for the gluon-fusion process $gg \rightarrow H^+H^-$ at NLO QCD [9] by a new and complete derivation in the heavy-top limit (HTL) and by extending the vector-boson fusion (VBF) $qq \rightarrow qqH^+H^-$ [10] to the NLO level as well. We perform a detailed analysis of all related uncertainties. Section 2 introduces the 2HDM of type I and the set-up and scenarios used in our work. In Section 3 we discuss the Drell–Yan-like process at NLO, while in Section 4 we elaborate on the loop-induced gluon-fusion process $gg \rightarrow H^+H^-$ and discuss the NLO QCD corrections. Section 5 describes our calculation of the VBF process and the related QCD corrections at NLO. In Section 6, we present our results with the full uncertainties of the combined scale and PDF+ α_s errors. In Section 7, we conclude.

2 The Two-Higgs Doublet Model

The 2HDM extends the SM by a second Higgs isospin-doublet with the same hypercharge [5, 6]. We elaborate on the 2HDM version with a softly broken \mathbb{Z}_2 symmetry which transforms the two Higgs doublets $\Phi_{1,2}$ as $\Phi_1 \rightarrow -\Phi_1$ and $\Phi_2 \rightarrow \Phi_2$. Introducing two $SU(2)_L$ Higgs doublets with hypercharge $Y = +1$, the most general $SU(2)_L \times U(1)_Y$ invariant Higgs potential with a softly broken \mathbb{Z}_2 symmetry reads

$$\begin{aligned} V = & m_{11}^2 |\Phi_1|^2 + m_{22}^2 |\Phi_2|^2 - m_{12}^2 (\Phi_1^\dagger \Phi_2 + h.c.) + \frac{\lambda_1}{2} (\Phi_1^\dagger \Phi_1)^2 + \frac{\lambda_2}{2} (\Phi_2^\dagger \Phi_2)^2 + \lambda_3 (\Phi_1^\dagger \Phi_1)(\Phi_2^\dagger \Phi_2) \\ & + \lambda_4 (\Phi_1^\dagger \Phi_2)(\Phi_2^\dagger \Phi_1) + \frac{\lambda_5}{2} [(\Phi_1^\dagger \Phi_2)^2 + h.c.] . \end{aligned} \quad (1)$$

We are working in the CP-conserving 2HDM, so that the three squared mass parameters, m_{11}^2 , m_{22}^2 and m_{12}^2 , and the five coupling parameters λ_i ($i = 1, \dots, 5$) are real. A discrete \mathbb{Z}_2 symmetry (softly broken by the term proportional to m_{12}^2) is introduced so that tree-level flavour-changing neutral currents (FCNC) are absent. When the \mathbb{Z}_2 symmetry is extended to the fermion sector, the families of same-charge fermions are enforced to couple to a single doublet so that tree-level FCNCs will be eliminated [6, 11]. This allows for four different types of fermionic doublet couplings. The associated types of the 2HDM are named type I, type II, lepton-specific and flipped. The emerging couplings of the fermions normalized to the SM couplings can be found in Ref. [6].

¹Recently, also a calculation of the Drell–Yan-like process for charged-Higgs pair production at *approximate* $N^2\text{LO}$ and $N^3\text{LO}$ was published [8].

After electroweak symmetry breaking, the Higgs isospin-doublets Φ_i ($i = 1, 2$) can be decomposed in their vacuum expectation values (vevs) v_i , the charged complex fields ϕ_i^+ , and the real neutral CP-even (ρ_i) and CP-odd (η_i) fields,

$$\Phi_1 = \begin{pmatrix} \phi_1^+ \\ \frac{v_1 + \rho_1 + i\eta_1}{\sqrt{2}} \end{pmatrix} \quad \text{and} \quad \Phi_2 = \begin{pmatrix} \phi_2^+ \\ \frac{v_2 + \rho_2 + i\eta_2}{\sqrt{2}} \end{pmatrix}. \quad (2)$$

The mass matrices can be derived from the bilinear Higgs-field terms in the potential. The diagonalization is achieved by the orthogonal transformations

$$\begin{aligned} \begin{pmatrix} \rho_1 \\ \rho_2 \end{pmatrix} &= R(\alpha) \begin{pmatrix} H \\ h \end{pmatrix}, \\ \begin{pmatrix} \eta_1 \\ \eta_2 \end{pmatrix} &= R(\beta) \begin{pmatrix} G^0 \\ A \end{pmatrix}, \\ \begin{pmatrix} \phi_1^\pm \\ \phi_2^\pm \end{pmatrix} &= R(\beta) \begin{pmatrix} G^\pm \\ H^\pm \end{pmatrix}. \end{aligned} \quad (3)$$

This results in five physical Higgs states, two neutral light and heavy CP-even, h, H , a neutral CP-odd, A , and two charged Higgs bosons, H^\pm , where by definition, $M_h < M_H$. The massless would-be Goldstone bosons G^\pm and G^0 are absorbed by the massive gauge bosons W, Z giving rise to their longitudinal components. The corresponding rotation matrices involve the mixing angles $\theta = \alpha$ and β , respectively,

$$R(\theta) = \begin{pmatrix} \cos \theta & -\sin \theta \\ \sin \theta & \cos \theta \end{pmatrix}. \quad (4)$$

The mixing angle β is related to the two vevs,

$$\tan \beta = \frac{v_2}{v_1}, \quad (5)$$

with $v_1^2 + v_2^2 = v^2 = 1/(\sqrt{2}G_F) \approx (246 \text{ GeV})^2$ determined by the Fermi constant G_F . Introducing the auxiliary parameters

$$M^2 \equiv \frac{m_{12}^2}{s_\beta c_\beta}, \quad \lambda_{345} \equiv \lambda_3 + \lambda_4 + \lambda_5, \quad (6)$$

the mixing angle α can be derived as [12]

$$\tan 2\alpha = \frac{s_{2\beta}(M^2 - \lambda_{345}v^2)}{c_\beta^2(M^2 - \lambda_1 v^2) - s_\beta^2(M^2 - \lambda_2 v^2)}, \quad (7)$$

adopting the short-hand notation $s_x \equiv \sin x$ etc.

Using the minimum conditions of the potential, the following set of seven independent input parameters of the model can be used,

$$M_h, M_{H^\pm}, \tan \beta, \lambda_1, \lambda_3, \lambda_4, \lambda_5, \quad (8)$$

next to the SM vev derived from the Fermi constant. In our analysis, we focus on the 2HDM type I, where the couplings of each physical Higgs boson to the up- and down-type fermions are equal. We study two scenarios, one for small and one for large values of $\tan \beta$. The charged Higgs mass M_{H^\pm} for each scenario is varied between 300 GeV and 2 TeV, while the remaining five input parameters, $\{M_h, \lambda_1, \lambda_3, \lambda_4, \lambda_5\}$, are chosen to be constant. The variation of M_{H^\pm} consequently implies a variation in the dependent parameters, i.e. of the mass parameters, remaining physical BSM masses and the mixing angle $\{m_{11}^2, m_{22}^2, m_{12}^2, M_h, M_A, \alpha\}$. For each value of M_{H^\pm} this new set of dependent parameters is determined via an iteration to ensure that the value of the quartic coupling λ_2 is constant too. By fixing the quartic couplings we ensure that the chosen scenarios are able to fulfill all relevant theoretical and experimental constraints over a maximal variation of the charged Higgs mass which we check for with **ScannerS** [13] linked with **HiggsBounds** [14]. Our chosen scenario for $\tan \beta = 2$ is constrained by electroweak precision data and flavour observables to $M_{H^\pm} \gtrsim 344$ GeV, while the scenario with $\tan \beta = 20$ is allowed by all relevant constraints over the full charged Higgs mass range.

The two scenarios of the 2HDM type I we use in our numerical analysis are given by the following set of input parameters

scenario 1:

$$\begin{aligned} \tan \beta &= 2, & \lambda_1 &= 6.499, & \lambda_3 &= -1.459, \\ & & \lambda_4 &= 1.106, & \lambda_5 &= -0.3621, \end{aligned} \quad (9)$$

scenario 2:

$$\begin{aligned} \tan \beta &= 20, & \lambda_1 &= 2.651, & \lambda_3 &= 0.2799, \\ & & \lambda_4 &= 2.392, & \lambda_5 &= 2.412, \end{aligned} \quad (10)$$

while the light scalar Higgs mass is fixed as $M_h = 125$ GeV.

3 Drell–Yan like H^+H^- Production

Within the type-I 2HDM the bottom Yukawa couplings are not enhanced so that the contribution of bottom-Yukawa-induced processes, see Fig. 1b, starting from a $b\bar{b}$ state are tiny (at the few per-mille level) compared to the leading Drell–Yan-like contributions emerging from

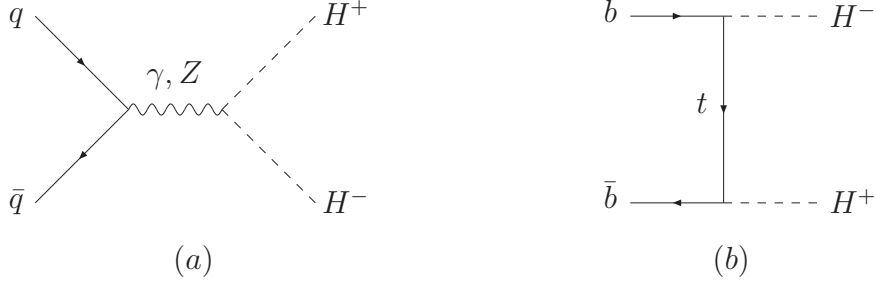


Figure 1: *Typical diagrams contributing to $q\bar{q} \rightarrow V^* \rightarrow H^+H^-$ at lowest order: (a) Drell–Yan-like contribution, (b) bottom-Yukawa induced contribution.*

s -channel photon and Z -boson exchange, see Fig. 1a. Therefore, we are neglecting the bottom-Yukawa-induced part in the following. The lowest-order partonic cross section can be expressed as [15]

$$\hat{\sigma}_{\text{LO}}(q\bar{q} \rightarrow H^+H^-) = \frac{\pi\alpha^2\beta^3}{9Q^2} \left\{ e_q^2 + 2\frac{e_q v_q v_H}{1 - \frac{M_Z^2}{Q^2}} + \frac{(v_q^2 + a_q^2)v_H}{\left(1 - \frac{M_Z^2}{Q^2}\right)^2} \right\}, \quad (11)$$

where $\beta = \sqrt{1 - 4\frac{M_{H^\pm}^2}{Q^2}}$ denotes the usual two-body phase-space factor and v_q (a_q) are the (axial) vector couplings of the quarks q to the vector bosons γ, Z and v_H the one of the charged Higgs bosons,

$$v_q = \frac{2I_{3q} - 4e_q s_W^2}{2s_W c_W}, \quad a_q = \frac{2I_{3q}}{2s_W c_W}, \quad v_H = \frac{1 - 2s_W^2}{2}, \quad (12)$$

and $I_{3q}(e_q)$ denotes the third isospin component (electric charge) of the quarks q . The sine of the Weinberg angle has been defined in terms of the W, Z masses, $s_W^2 = 1 - M_W^2/M_Z^2$. The partonic center-of-mass energy squared \hat{s} coincides at lowest order with the squared invariant mass $Q^2 = M_{H^+H^-}^2$ of the charged Higgs pair, $\hat{s} = Q^2$. The hadronic cross section can be obtained from convolving eq. (11) with the corresponding (anti)quark densities of the protons,

$$\sigma_{\text{LO}}(pp \rightarrow H^+H^-) = \int_{\tau_0}^1 d\tau \sum_q \frac{d\mathcal{L}^{q\bar{q}}}{d\tau} \hat{\sigma}_{\text{LO}}(Q^2 = \tau s), \quad (13)$$

with $\tau_0 = 4M_{H^\pm}^2/s$ and s the squared total hadronic c.m. energy.

The QCD corrections are identical to the corresponding corrections to the Drell–Yan process,

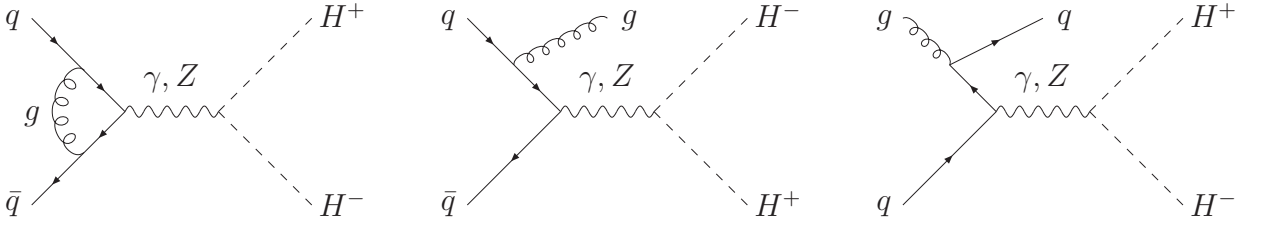


Figure 2: *Typical diagrams contributing to $q\bar{q} \rightarrow V^* \rightarrow H^+H^-$ at NLO.*

see Fig. 2. They modify the lowest order cross section in the following way [16]:

$$\begin{aligned} \sigma(pp \rightarrow H^+H^-) &= \sigma_{\text{LO}} + \Delta\sigma_{q\bar{q}} + \Delta\sigma_{qg}, \\ \Delta\sigma_{q\bar{q}} &= \frac{\alpha_s(\mu_R)}{\pi} \int_{\tau_0}^1 d\tau \sum_q \frac{d\mathcal{L}^{q\bar{q}}}{d\tau} \int_{\tau_0/\tau}^1 dz \hat{\sigma}_{\text{LO}}(Q^2 = \tau z s) \omega_{q\bar{q}}(z), \\ \Delta\sigma_{qg} &= \frac{\alpha_s(\mu_R)}{\pi} \int_{\tau_0}^1 d\tau \sum_{q,\bar{q}} \frac{d\mathcal{L}^{qg}}{d\tau} \int_{\tau_0/\tau}^1 dz \hat{\sigma}_{\text{LO}}(Q^2 = \tau z s) \omega_{qg}(z), \end{aligned} \quad (14)$$

with the coefficient functions

$$\begin{aligned} \omega_{q\bar{q}}(z) &= -P_{qq}(z) \log \frac{\mu_F^2}{\tau s} + \frac{4}{3} \left\{ 2[\zeta_2 - 2]\delta(1-z) + 4\mathcal{D}_1(z) - 2(1+z) \log(1-z) \right\}, \\ \omega_{qg}(z) &= -\frac{1}{2}P_{qg}(z) \log \left(\frac{\mu_F^2}{(1-z)^2 \tau s} \right) + \frac{1}{8} \left\{ 1 + 6z - 7z^2 \right\}, \end{aligned} \quad (15)$$

where $\mu_R(\mu_F)$ denotes the renormalization (factorization) scale and the Altarelli–Parisi splitting functions are given by [17]

$$\begin{aligned} P_{qq}(z) &= \frac{4}{3} \left\{ 2\mathcal{D}_0(z) - 1 - z + \frac{3}{2}\delta(1-z) \right\}, \\ P_{qg}(z) &= \frac{1}{2} \left\{ z^2 + (1-z)^2 \right\}. \end{aligned} \quad (16)$$

The plus distributions $\mathcal{D}_i(z)$ involved in the expressions above read

$$\mathcal{D}_i(z) = \left(\frac{\log^i(1-z)}{1-z} \right)_+ \quad (i = 0, 1, \dots). \quad (17)$$

The parton luminosity functions are given by

$$\begin{aligned} \frac{d\mathcal{L}^{q\bar{q}}}{d\tau} &= \int_{\tau}^1 \frac{dx}{x} [q(x, \mu_F^2) \bar{q}(\tau/x, \mu_F^2) + \bar{q}(x, \mu_F^2) q(\tau/x, \mu_F^2)], \\ \frac{d\mathcal{L}^{qg}}{d\tau} &= \int_{\tau}^1 \frac{dx}{x} [q(x, \mu_F^2) g(\tau/x, \mu_F^2) + g(x, \mu_F^2) q(\tau/x, \mu_F^2)]. \end{aligned} \quad (18)$$

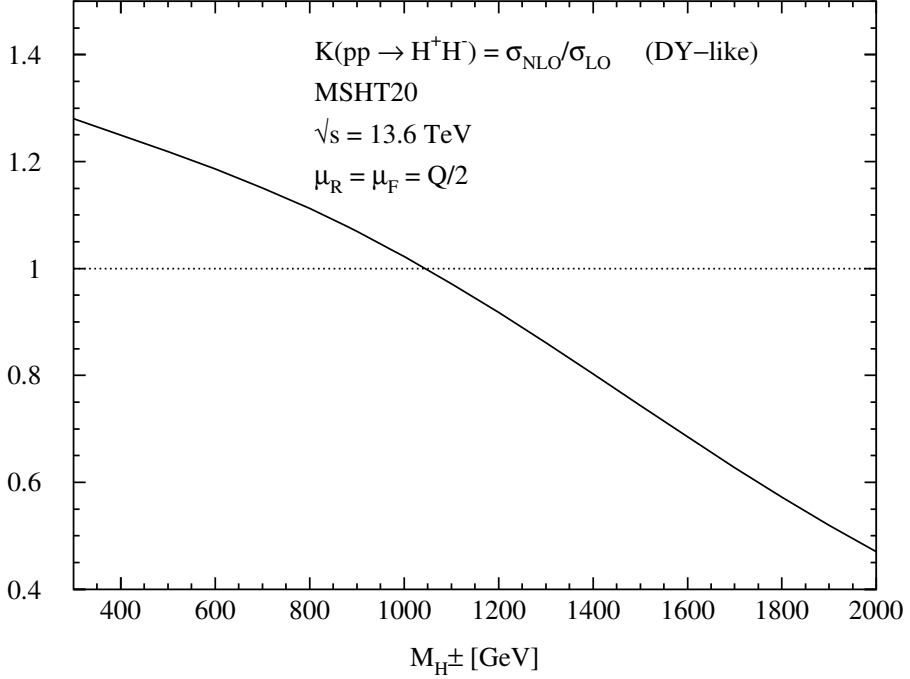


Figure 3: The K factor, defined as the ratio $\sigma_{\text{NLO}}/\sigma_{\text{LO}}$, for the Drell–Yan like cross section of charged-Higgs pair production as a function of the charged Higgs mass. It is the same in both 2HDM scenarios. The MSHT20lo-as130 and MSHT20nlo-as118 parton densities (PDFs) [18] were used for the LO and NLO cross sections, respectively, for a consistent definition of the K factor. The cross section is independent of $\tan\beta$ at LO and NLO.

The QCD corrections to the Drell–Yan-like charged-Higgs pair production are of more moderate size, i.e. modifying the cross section by up to about 30%, when adopting the scale choice $\mu_R = \mu_F = Q/2$, where Q is the invariant mass of the charged Higgs pair, as is shown in Fig. 3. However, for large charged Higgs masses the QCD corrections decrease the cross section by about 50%, but this effects depends strongly on the NLO/LO PDF sets used in this calculation. Since the cross section at leading order (LO) and NLO is independent of $\tan\beta$, the K factor and the related uncertainties are independent of $\tan\beta$ as well. The scale uncertainties were determined by the usual 7-point variation of the factorization and renormalization scales. This results in residual generic theoretical uncertainties of up to about 5% at the NLO level with a significant reduction from the LO prediction, see Fig. 4. The missing overlap between the LO and NLO error bands indicates that the LO uncertainties are not valid in quantitative terms. However, the significant reduction of the scale dependence from LO to NLO indicates the perturbative reliability of the NLO predictions and its residual uncertainties that amount to 3–5%. The Drell–Yan like charged-Higgs pair production process is entirely mediated by

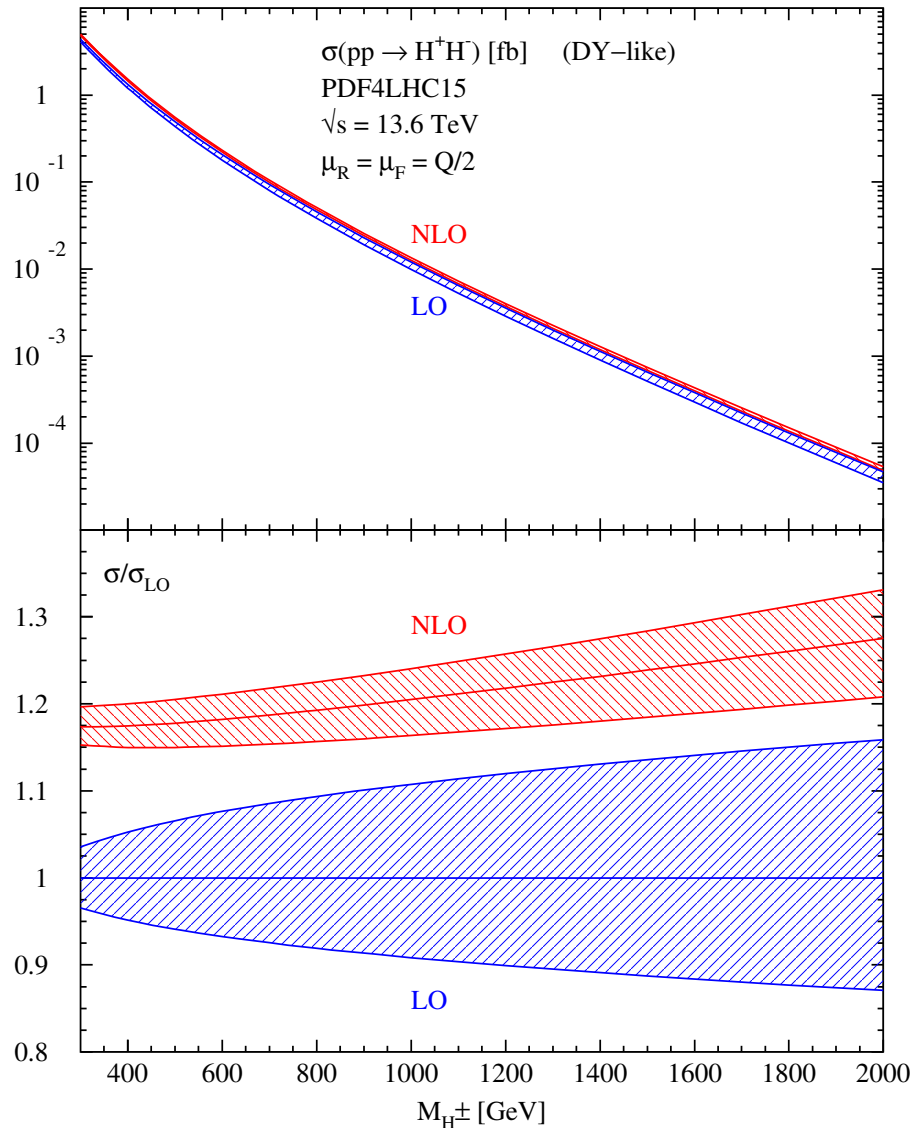


Figure 4: *Drell-Yan like cross section of charged-Higgs pair production as a function of the charged Higgs mass with scale uncertainties. The PDF4LHC15 parton densities [19] have been used for the LO and NLO cross sections.*

gauge couplings and thus independent of $\tan\beta$ at LO and NLO.

4 H^+H^- Production in Gluon Fusion

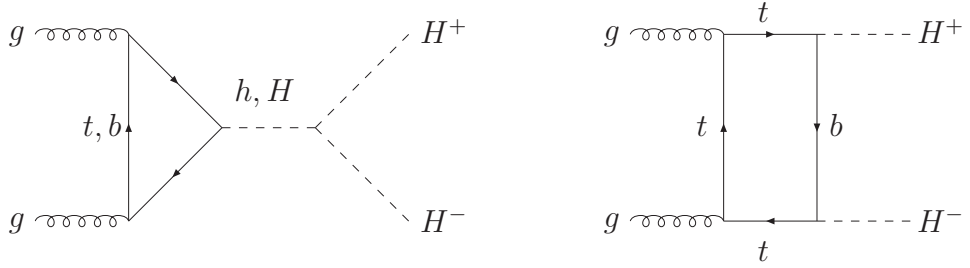


Figure 5: *Typical diagrams contributing to $gg \rightarrow H^+H^-$ at lowest order.*

Charged-Higgs pair production via gluon fusion is a loop-induced process that is mediated by mixed top/bottom triangle and box diagrams at LO, see Fig. 5. Generically the partonic LO cross section can be expressed as [20]

$$\hat{\sigma}_{\text{LO}}(gg \rightarrow H^+H^-) = \int_{\hat{t}_-}^{\hat{t}_+} d\hat{t} \frac{G_F^2 \alpha_s^2(\mu_R)}{256(2\pi)^3} \{ |C_\Delta F_\Delta + F_\square|^2 + |G_\square|^2 + |H_\square|^2 \}. \quad (19)$$

The Mandelstam variables for the parton process are given by

$$\hat{s} = Q^2, \quad \hat{t}/\hat{u} = -\frac{1}{2} [Q^2 - 2M_{H^\pm}^2 \mp Q^2 \beta \cos\theta], \quad (20)$$

where Q^2 denotes the squared invariant charged-Higgs pair mass, $Q^2 = M_{H^+H^-}^2$, and θ is the scattering angle in the partonic center-of-mass system, while

$$\beta = \sqrt{1 - 4 \frac{M_{H^\pm}^2}{Q^2}}. \quad (21)$$

The integration limits

$$\hat{t}_\pm = -\frac{1}{2} [Q^2 - 2M_{H^\pm}^2 \mp Q^2 \beta] \quad (22)$$

in Eq. (19), correspond to $\cos\theta = \pm 1$. The scale parameter μ_R (μ_F) is the renormalization (factorization) scale. The complete dependence on the fermion masses is contained in the functions F_Δ , F_\square , G_\square and H_\square . The full expressions of the form factors F_Δ , F_\square , G_\square , H_\square , including the exact dependence on the fermion masses, can be found in Ref. [20].

The coupling C_Δ in general, and the form factors F_Δ , F_\square , G_\square , H_\square in the HTL are given by

$$C_\Delta = \sum_{H_i=h,H} \frac{\lambda_{H_i H^+ H^-}}{\hat{s} - M_{H_i}^2}, \quad F_\Delta \rightarrow \frac{2}{3} g_t^{H_i}, \quad F_\square \rightarrow \frac{2}{3 \tan^2 \beta}, \quad G_\square, H_\square \rightarrow 0, \quad (23)$$

where the trilinear scalar Higgs couplings to charged Higgs states are given by

$$\lambda_{hH^+H^-} = (M_h^2 + 2M_{H^\pm}^2 - 2M^2)s_{\beta-\alpha} + 2c_{\beta-\alpha}\cot(2\beta)(M_h^2 - M^2), \quad (24)$$

$$\lambda_{HH^+H^-} = (M_H^2 + 2M_{H^\pm}^2 - 2M^2)c_{\beta-\alpha} - 2s_{\beta-\alpha}\cot(2\beta)(M_H^2 - M^2). \quad (25)$$

and the neutral Higgs Yukawa-coupling factors read

$$g_t^h = \frac{s_\alpha}{s_\beta}, \quad g_t^H = \frac{c_\alpha}{s_\beta}. \quad (26)$$

The expressions in the HTL can be obtained from the effective Lagrangian

$$\mathcal{L}_{\text{eff}} = \frac{\alpha_s}{24\pi} G^{a\mu\nu} G_{\mu\nu}^a \log\left(\frac{2|\Phi_2|^2}{v_2^2}\right) \left(1 + \frac{11}{4}\frac{\alpha_s}{\pi}\right), \quad (27)$$

including NLO QCD corrections², where $G^{a\mu\nu}$ denotes the gluon field strength tensor, and the second Higgs doublet Φ_2 of Eq. (2) is used. Expanding the Higgs fields of Φ_2 according to Eq. (3), one arrives at the relevant part of the effective Lagrangian for this process

$$\mathcal{L}_{\text{eff}} = \frac{\alpha_s}{12\pi v} G^{a\mu\nu} G_{\mu\nu}^a \left\{ h \frac{s_\alpha}{s_\beta} + H \frac{c_\alpha}{s_\beta} + \frac{H^+H^-}{v \tan^2 \beta} + \dots \right\} \left(1 + \frac{11}{4}\frac{\alpha_s}{\pi}\right). \quad (28)$$

Using this effective Lagrangian, the NLO QCD corrections can be approximated by the ones obtained in the HTL (see Fig. 6), but convolved with the full LO partonic cross section kernel of Eq. (19),

$$\sigma_{\text{NLO}}(pp \rightarrow H^+H^- + X) = \sigma_{\text{LO}} + \Delta\sigma_{\text{virt}} + \Delta\sigma_{gg} + \Delta\sigma_{gq} + \Delta\sigma_{q\bar{q}}, \quad (29)$$

with the individual contributions

$$\begin{aligned} \sigma_{\text{LO}} &= \int_{\tau_0}^1 d\tau \frac{d\mathcal{L}^{gg}}{d\tau} \hat{\sigma}_{\text{LO}}(Q^2 = \tau s), \\ \Delta\sigma_{\text{virt}} &= \frac{\alpha_s(\mu_R)}{\pi} \int_{\tau_0}^1 d\tau \frac{d\mathcal{L}^{gg}}{d\tau} \hat{\sigma}_{\text{LO}}(Q^2 = \tau s) \left\{ \pi^2 + \frac{11}{2} + \frac{33 - 2N_F}{6} \log \frac{\mu_R^2}{Q^2} \right\}, \\ \Delta\sigma_{gg} &= \frac{\alpha_s(\mu_R)}{\pi} \int_{\tau_0}^1 d\tau \frac{d\mathcal{L}^{gg}}{d\tau} \int_{\tau_0/\tau}^1 \frac{dz}{z} \hat{\sigma}_{\text{LO}}(Q^2 = z\tau s) \left\{ -zP_{gg}(z) \log \frac{\mu_F^2}{\tau s} \right. \\ &\quad \left. - \frac{11}{2}(1-z)^3 + 6[1+z^4 + (1-z)^4] \mathcal{D}_1(z) \right\}, \\ \Delta\sigma_{gq} &= \frac{\alpha_s(\mu_R)}{\pi} \int_{\tau_0}^1 d\tau \sum_{q,\bar{q}} \frac{d\mathcal{L}^{gq}}{d\tau} \int_{\tau_0/\tau}^1 \frac{dz}{z} \hat{\sigma}_{\text{LO}}(Q^2 = z\tau s) \left\{ -\frac{z}{2}P_{gq}(z) \log \frac{\mu_F^2}{\tau s(1-z)^2} \right. \\ &\quad \left. + \frac{2}{3}z^2 - (1-z)^2 \right\}, \\ \Delta\sigma_{q\bar{q}} &= \frac{\alpha_s(\mu_R)}{\pi} \int_{\tau_0}^1 d\tau \sum_q \frac{d\mathcal{L}^{q\bar{q}}}{d\tau} \int_{\tau_0/\tau}^1 \frac{dz}{z} \hat{\sigma}_{\text{LO}}(Q^2 = z\tau s) \frac{32}{27}(1-z)^3, \end{aligned} \quad (30)$$

²The NLO QCD corrections to the effective Lagrangian are the same for the charged and neutral states.

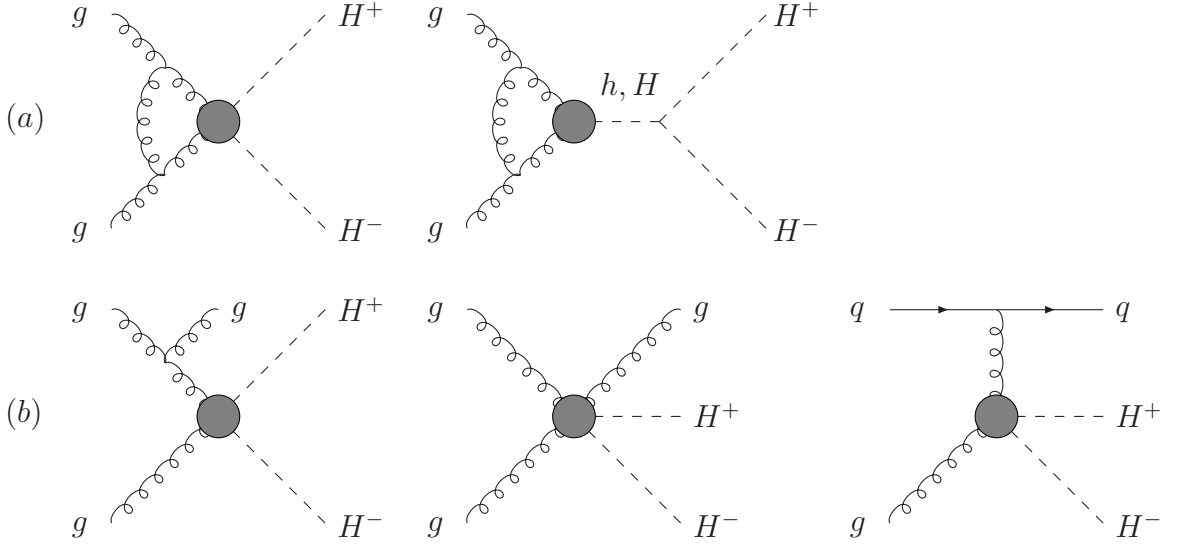


Figure 6: *Typical effective diagrams contributing to the (a) virtual and (b) real corrections to charged Higgs-boson pair production via gluon fusion, where for the blobs, the effective Feynman rules derived from the Lagrangian in Eq. (28) are used.*

where

$$\tau_0 = 4 \frac{M_{H^\pm}^2}{s}. \quad (31)$$

The objects $P_{gg}(z), P_{gq}(z)$ denote the Altarelli–Parisi splitting functions [17]

$$\begin{aligned} P_{gg}(z) &= 6 \left\{ \mathcal{D}_0(z) + \frac{1}{z} - 2 + z(1-z) \right\} + \frac{33 - 2N_F}{6} \delta(1-z), \\ P_{gq}(z) &= \frac{4}{3} \frac{1 + (1-z)^2}{z}, \end{aligned} \quad (32)$$

with $N_F = 5$ in our case. The parton–parton luminosities $d\mathcal{L}^{ij}/d\tau$ are given in Eq. (18) and

$$\frac{d\mathcal{L}^{gg}}{d\tau} = \int_\tau^1 \frac{dx}{x} g(x, \mu_F^2) g(\tau/x, \mu_F^2). \quad (33)$$

The results above are adopted from the corresponding calculation in the single-Higgs case [21] and neutral Higgs-boson pair production [22] in the HTL. Compared to the neutral-Higgs pair production there is no one-particle reducible contribution with gluon exchange in the t -channel between two of the effective vertices here, so that the virtual corrections are simpler.

The QCD corrections to the gluon-fusion cross section are large³ i.e. increasing the cross section by up to about 80% for the central scale choice of half the invariant charged-Higgs pair

³We find reasonable agreement with the approximate results of Ref. [9].

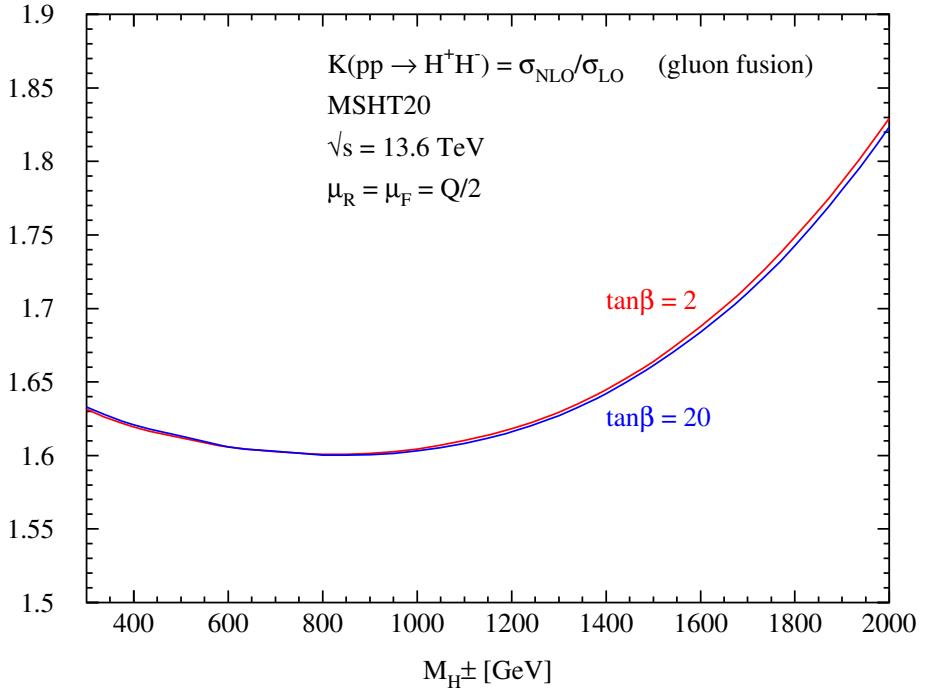


Figure 7: The K factor of the gluon-fusion cross section describing charged-Higgs pair production as a function of the charged Higgs mass for the two 2HDM scenarios. The `MSHT20lo_as130` and `MSHT20nlo_as118` PDFs [18] were adopted for the LO and NLO cross sections, respectively, for the consistent definition of the K factor.

mass, see Fig. 7. Thus their inclusion is highly relevant to arrive at a reliable prediction of the production rate⁴. The relative QCD corrections develop only a minor dependence on the value of $\tan\beta$, while the inclusive cross section exhibits a strong $\tan\beta$ dependence, see Figs. 8, 9. The residual renormalization and factorization scale dependence were determined by the 7-point method. The residual uncertainties at NLO appear to be at the level of up to 20–25% for the scale choice of half the invariant charged-Higgs pair mass, see Figs. 8, 9. Also in this case we do not observe an overlap between the LO and NLO scale variation bands so that the LO uncertainty estimate is not reliable. This is in line with the observations in neutral-Higgs pair production via gluon fusion [22].

⁴The neglected quark-mass effects at NLO in the HTL are expected at the 20–30% level in line with the observations for the neutral-Higgs pair production via gluon fusion [23].

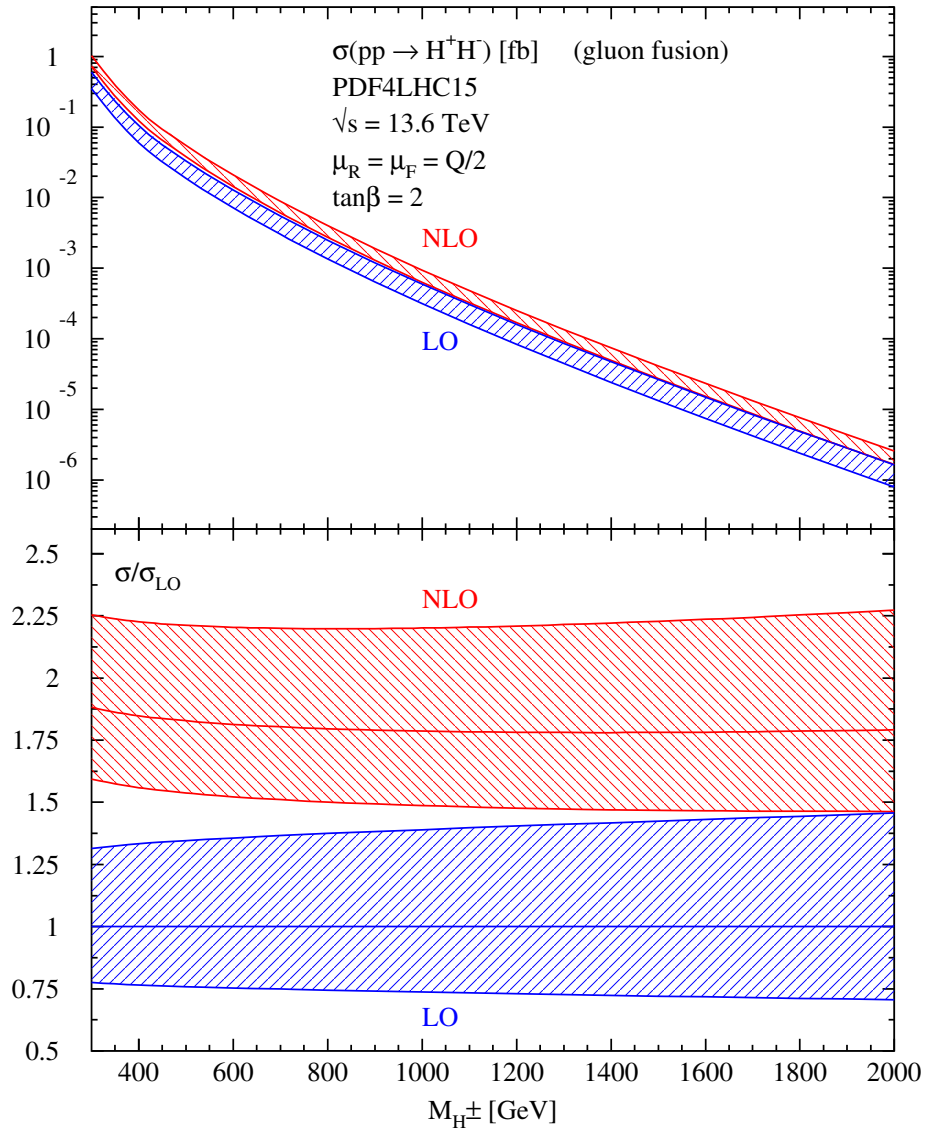


Figure 8: Gluon-fusion cross section of charged-Higgs pair production as a function of the charged Higgs mass with scale uncertainties for the scenario with $\tan\beta = 2$. The PDF4LHC15 PDFs [19] were used for the LO and NLO cross sections.

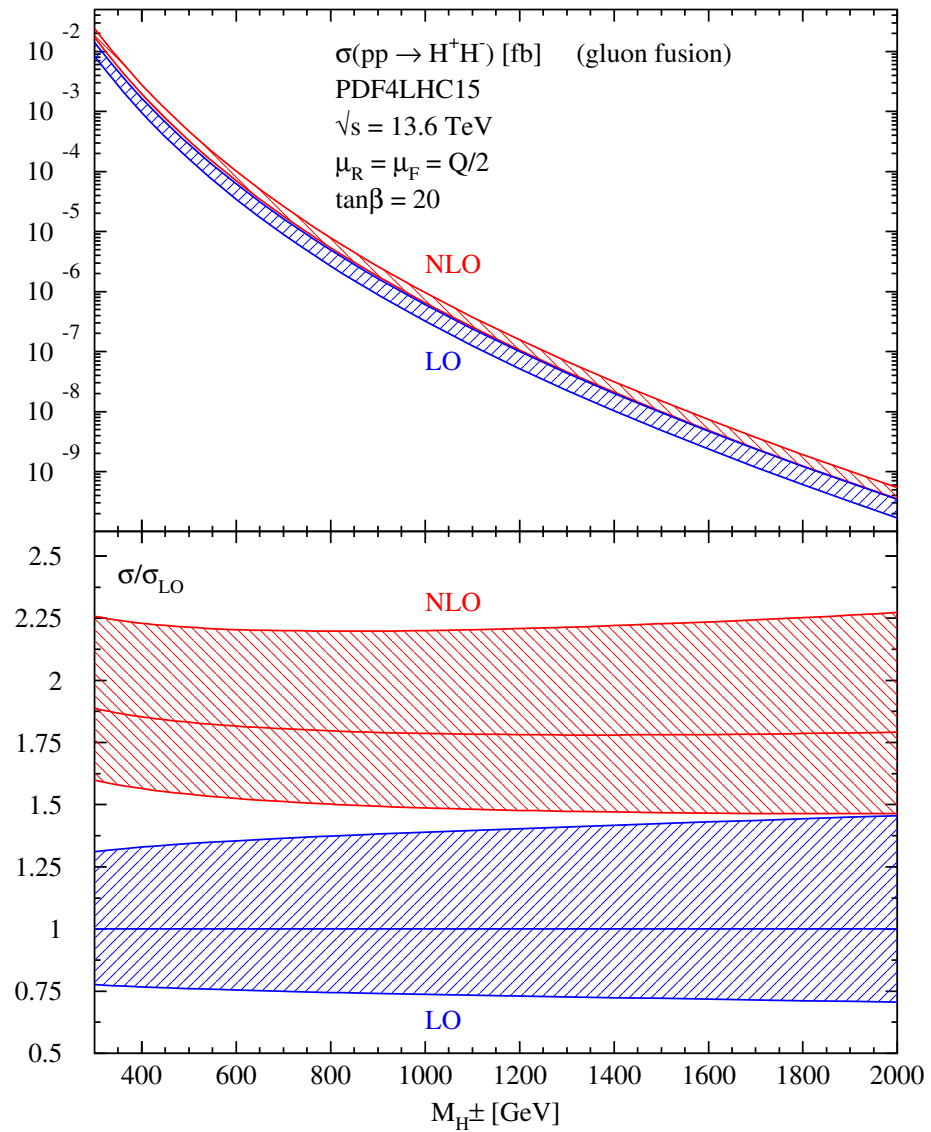


Figure 9: The same as Fig. 8 but for $\tan\beta = 20$.

5 H^+H^- Production in Vector-Boson Fusion

Charged-Higgs pairs can also be produced via VBF, where the Higgs pair emerges from photons, Z bosons or W bosons emitted from the incoming quarks and antiquarks, see Fig. 10. We are

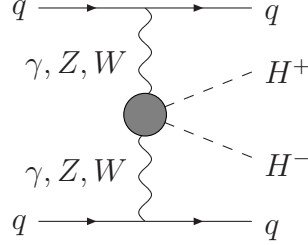


Figure 10: *Generic diagram of vector-boson fusion at LO. The blob contains all subdiagrams of the processes $V_1V_2 \rightarrow H^+H^-$ with $V_{1,2} = \gamma, Z, W$.*

treating this process in the structure-function approach (SFA) that neglects interference terms in the case of identical incoming quarks that arise between diagrams of the type of Fig. 10 with the corresponding one with crossed quark lines in the final state. In this approach, the squared matrix element of the process can be expressed as

$$|\mathcal{M}|^2 = 4q_1^2 q_2^2 \sum_{V_1, \dots, 4 = \gamma, Z} \frac{g_{V_1} g_{V_2} g_{V_3} g_{V_4}}{(q_1^2 - M_{V_1}^2)(q_2^2 - M_{V_2}^2)(q_1^2 - M_{V_3}^2)(q_2^2 - M_{V_4}^2)} W_{V_1 V_3}^{\mu\rho} W_{V_2 V_4}^{\nu\sigma} \mathcal{M}_{V_1 V_2}^{\mu\nu} \mathcal{M}_{V_3 V_4}^{*\rho\sigma} + \frac{4q_1^2 q_2^2}{(q_1^2 - M_W^2)^2 (q_2^2 - M_W^2)^2} \sum_{WW' = W^+W^-, W^-W^+} W_{WW}^{\mu\rho} W_{W'W'}^{\nu\sigma} \mathcal{M}_{WW'}^{\mu\nu} \mathcal{M}_{WW'}^{*\rho\sigma}, \quad (34)$$

where $q_{1,2}^2$ denote the squared momenta of the individual vector bosons at the corresponding proton leg and the gauge-coupling factors are given by

$$g_\gamma = e, \quad g_Z = \frac{M_Z}{2v}, \quad g_W = \frac{M_W}{2v}. \quad (35)$$

The matrix elements of the subprocesses $V_1(q_1)V_2(q_2) \rightarrow H^+(p_1)H^-(p_2)$ ($V_{1,2} = \gamma, Z, W$), see

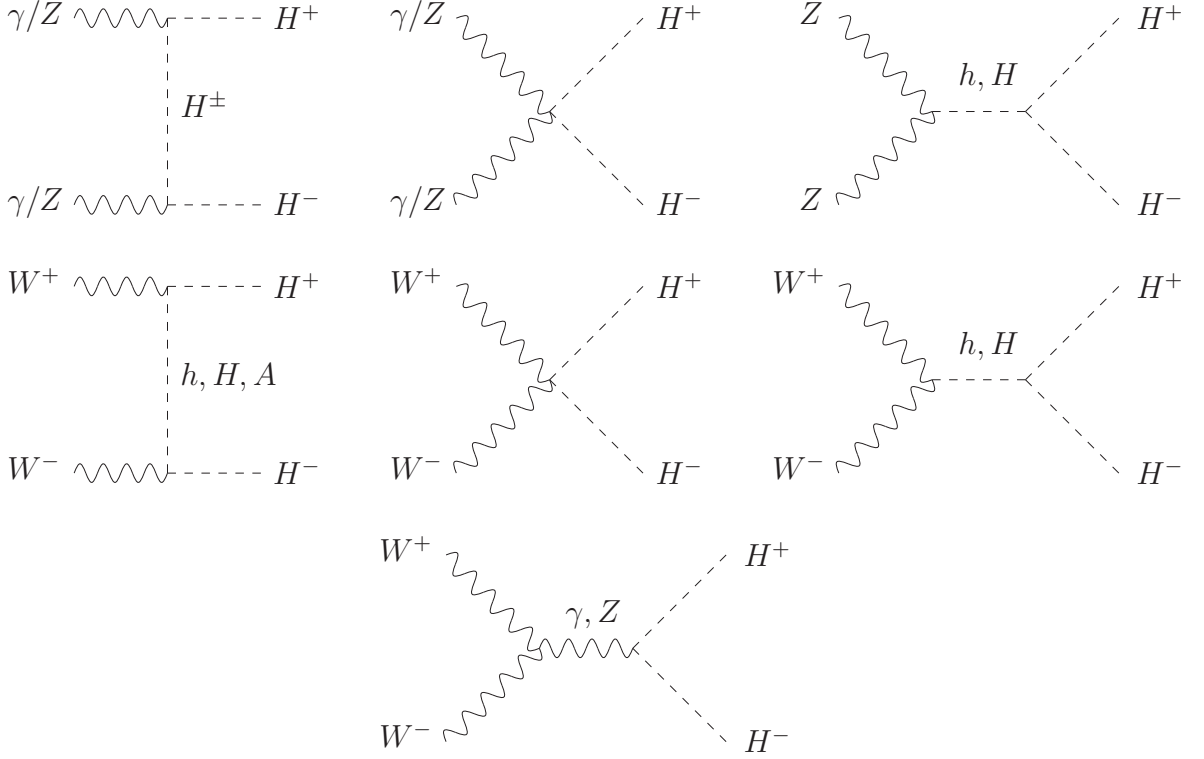


Figure 11: *Typical diagrams contributing to the subprocesses of charged-Higgs pair production via VBF.*

Fig. 11, can be cast into the form

$$\begin{aligned}
\mathcal{M}_{W^+W^-}^{\mu\nu} &= ig_W^2 \left\{ \sum_{\phi=h,H,A} \frac{|\tilde{g}_W^\phi|^2}{\tilde{t} - M_{H_i}^2} (q_1 - 2p_1)^\mu (q_2 - 2p_2)^\nu + 2g^{\mu\nu} \left[1 + \sum_{H_i=h,H} \frac{g_W^{H_i} \lambda_{H_i H^+ H^-}}{\tilde{s} - M_\phi^2} \right] \right\} \\
&\quad - \sum_{V=\gamma,Z} i \frac{g_{3V} g_V c_V}{\tilde{s} - M_V^2} \{ g^{\mu\nu} (p_1 - p_2) (q_1 - q_2) - (p_1 - p_2)^\mu (q_1 + q)^\nu + (p_1 - p_2)^\nu (q_2 + q)^\mu \} \\
\mathcal{M}_{V_1 V_2}^{\mu\nu} &= ig_{V_1} g_{V_2} \left\{ c_{V_1} c_{V_2} \left[\frac{(q_1 - 2p_1)^\mu (q_2 - 2p_2)^\nu}{\tilde{t} - M_{H^\pm}^2} + \frac{(q_1 - 2p_2)^\mu (q_2 - 2p_1)^\nu}{\tilde{u} - M_{H^\pm}^2} + 2g^{\mu\nu} \right] \right. \\
&\quad \left. + \delta_{V_1 Z} \delta_{V_2 Z} 2g^{\mu\nu} \sum_{H_i=h,H} g_V^{H_i} \frac{\lambda_{H_i H^+ H^-}}{\tilde{s} - M_{H_i}^2} \right\} \quad (V_{1,2} = \gamma, Z) \quad (36)
\end{aligned}$$

with $c_\gamma = 1$, $c_Z = 1 - 2s_W^2$, $\tilde{s} = (q_1 + q_2)^2$, $\tilde{t} = (p_1 - q_1)^2$ and $\tilde{u} = (p_1 - q_2)^2$. The other coupling factors are given by

$$g_{W/Z}^h = -\tilde{g}_W^H = s_{\beta-\alpha}, \quad g_{W/Z}^H = \tilde{g}_W^h = c_{\beta-\alpha}, \quad \tilde{g}_W^A = -i, \quad g_{3V} = \begin{cases} e & ; V = \gamma \\ 2\frac{M_W}{v}c_W & ; V = Z \end{cases} . \quad (37)$$

The contributing hadronic tensors are defined in terms of the usual structure functions $F_{1\dots 3}$ of deep inelastic lepton-nucleon scattering (where we need to distinguish between the corresponding vector-bosons)

$$W_{V_1 V_2}^{\mu\nu} = F_{1,V_1 V_2} \left(-g^{\mu\nu} + \frac{q^\mu q^\nu}{q^2} \right) - \frac{F_{2,V_1 V_2}}{xpq} \left(p^\mu - \frac{pq}{q^2} q^\mu \right) \left(p^\nu - \frac{pq}{q^2} q^\nu \right) - i \frac{F_{3,V_1 V_2}}{2pq} \epsilon^{\mu\nu\rho\sigma} p_\rho q_\sigma . \quad (38)$$

The 4-momentum p denotes the incoming *quark* momentum and q the *outgoing* gauge-boson momentum. The sums of Eq. (34) run over all contributing combinations of photon and Z exchanges as well as charged W exchanges (The neutral and charged vector-boson exchanges do not interfere.). The individual structure functions are defined as⁵

$$\begin{aligned} F_{1,V_1 V_2}(x, \mu_F^2) &= \sum_q (v_{q,V_1} v_{q,V_2} + a_{q,V_1} a_{q,V_2}) [q(x, \mu_F^2) + \bar{q}(x, \mu_F^2)], \\ F_{2,V_1 V_2}(x, \mu_F^2) &= 2x \sum_q (v_{q,V_1} v_{q,V_2} + a_{q,V_1} a_{q,V_2}) [q(x, \mu_F^2) + \bar{q}(x, \mu_F^2)], \\ F_{3,V_1 V_2}(x, \mu_F^2) &= 2 \sum_q (v_{q,V_1} a_{q,V_2} + a_{q,V_1} v_{q,V_2}) [-q(x, \mu_F^2) + \bar{q}(x, \mu_F^2)], \end{aligned} \quad (39)$$

where the electroweak coupling factors are given by

$$\begin{aligned} \gamma: \quad v_{q,\gamma} &= e_q, & a_{q,\gamma} &= 0, \\ Z: \quad v_{q,Z} &= 2I_{3q} - 4e_q s_W^2, & a_{q,Z} &= 2I_{3q}, \\ W: \quad v_{q,W} &= \sqrt{2}, & a_{q,W} &= \sqrt{2}. \end{aligned} \quad (40)$$

Finally, the differential cross section reads

$$d\sigma = \frac{\sum |\mathcal{M}|^2}{8s} \frac{dx_1 dx_2}{x_1 x_2} dPS_4, \quad (41)$$

with s denoting the squared hadronic c.m. energy and x_1, x_2 the two Bjorken- x values of the individual proton legs. The last factor dPS_4 is the suitably parametrized 4-particle phase space measure at the parton level. In line with the usual treatment of VBF in single-Higgs and neutral-Higgs pair production we are introducing a lower cut on the virtualities of the vector bosons, $Q_i^2 = -q_i^2 > 4 \text{ GeV}^2$ ($i = 1, 2$).

⁵For charged W -exchange contributions we do not take into account bottom PDFs, since they would lead to top quarks in the final state.

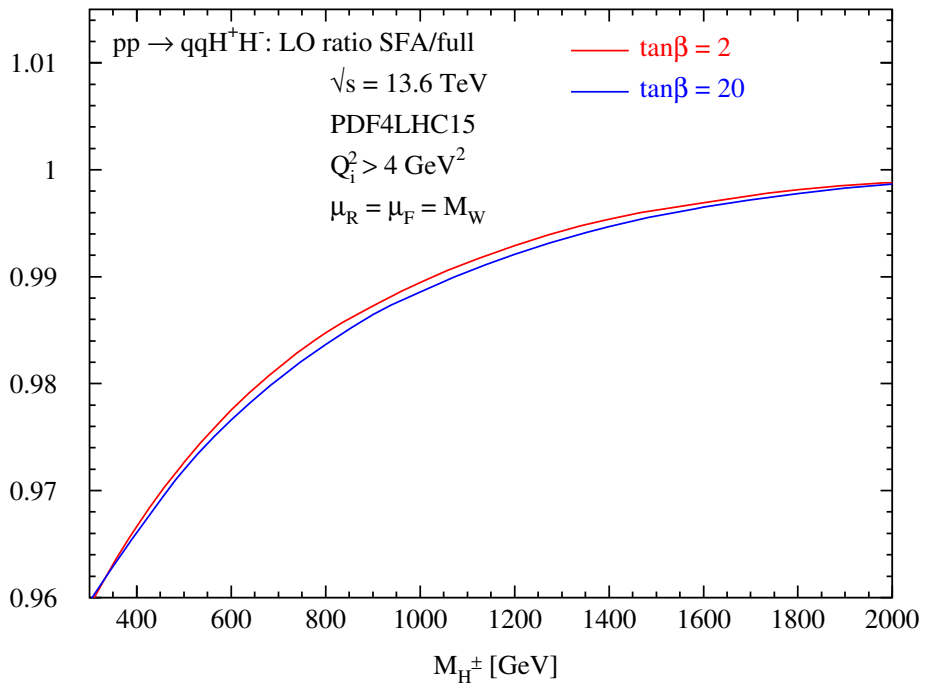


Figure 12: The ratio between the SFA and the full calculation of charged-Higgs pair production via VBF at LO for the two 2HDM scenarios of Eqs. (9,10) as a function of the charged Higgs mass. The PDF4LHC15 PDFs [19] were used for the LO cross sections.

For the two scenarios above, we have checked the validity of the SFA by comparing with the full calculation at LO. The LO calculation of the matrix element has been performed with SUSY–MadGraph [24] by omitting all non-VBF diagrams [25]⁶ The ratios between the SFA and the full calculation at LO are shown in Fig. 12 for a fixed scale choice $\mu_R = \mu_F = M_W$. We observe that the SFA agrees with the full calculation within about 3% for charged Higgs masses above about 400 GeV.

Very recently, a study has appeared on charged-Higgs pair production via photon fusion at the LHC [26], i.e. neglecting Z and W exchange diagrams. This approximation is compared with our full calculation at LO in Fig. 13, where the ratio of both calculations is depicted. It is clearly visible that photon-fusion only makes up less than 30% of the full results of charged-Higgs pair production. However, we did not include the experimental cuts the authors of Ref. [26] have applied, but the full cross section is significantly larger than just photon fusion so that the analysis of Ref. [26] requires more theoretical refinements.

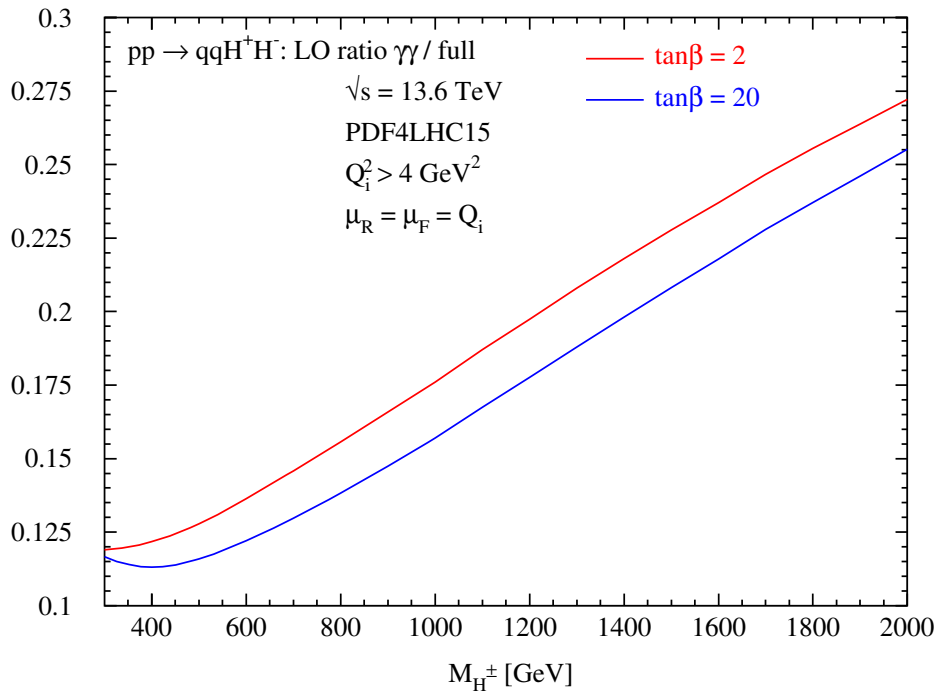


Figure 13: *The ratio between the pure photon-exchange contribution and the full calculation within the SFA of charged-Higgs pair production via VBF at LO for the two 2HDM scenarios of Eqs. (9,10) as a function of the charged Higgs mass. The PDF4LHC15 PDFs [19] were used for the LO cross sections.*

⁶Our comparison with the former LO calculation of Ref. [10] revealed several sources of discrepancies related to sign errors and incorrect definitions of electroweak couplings.

Within the structure-function approach the NLO QCD corrections can be implemented by shifting the structure functions by their known radiative corrections

$$F_{i,V_1V_2}(x, \mu_F^2) \rightarrow F_{i,V_1V_2}(x, \mu_F^2) + \Delta F_{i,V_1V_2}(x, \mu_F^2, Q^2) \quad (i = 1, 2, 3), \quad (42)$$

and expanding the full matrix element to NLO. The explicit NLO correction terms read

$$\begin{aligned} \Delta F_{1,V_1V_2}(x, \mu_F^2, Q^2) &= \frac{\alpha_s(\mu_R)}{\pi} \sum_q (v_{q,V_1} v_{q,V_2} + a_{q,V_1} a_{q,V_2}) \int_x^1 \frac{dy}{y} \left\{ \frac{2}{3} [q(y, \mu_F^2) + \bar{q}(y, \mu_F^2)] \right. \\ &\quad \left[-\frac{3}{4} P_{qq}(z) \log \frac{\mu_F^2 z}{Q^2} + (1 + z^2) \mathcal{D}_1(z) - \frac{3}{2} \mathcal{D}_0(z) \right. \\ &\quad \left. + 3 - \left(\frac{9}{2} + \frac{\pi^2}{3} \right) \delta(1 - z) \right] \\ &\quad + \frac{1}{4} g(y, \mu_F^2) \left[-2 P_{qg}(z) \log \frac{\mu_F^2 z}{Q^2(1 - z)} + 4z(1 - z) - 1 \right] \left. \right\}, \\ \Delta F_{2,V_1V_2}(x, \mu_F^2, Q^2) &= 2x \frac{\alpha_s(\mu_R)}{\pi} \sum_q (v_{q,V_1} v_{q,V_2} + a_{q,V_1} a_{q,V_2}) \int_x^1 \frac{dy}{y} \left\{ \frac{2}{3} [q(y, \mu_F^2) + \bar{q}(y, \mu_F^2)] \right. \\ &\quad \left[-\frac{3}{4} P_{qq}(z) \log \frac{\mu_F^2 z}{Q^2} + (1 + z^2) \mathcal{D}_1(z) - \frac{3}{2} \mathcal{D}_0(z) \right. \\ &\quad \left. + 3 + 2z - \left(\frac{9}{2} + \frac{\pi^2}{3} \right) \delta(1 - z) \right] \\ &\quad + \frac{1}{4} g(y, \mu_F^2) \left[-2 P_{qg}(z) \log \frac{\mu_F^2 z}{Q^2(1 - z)} + 8z(1 - z) - 1 \right] \left. \right\}, \\ \Delta F_{3,V_1V_2}(x, \mu_F^2, Q^2) &= \frac{\alpha_s(\mu_R)}{\pi} \sum_q 2(v_{q,V_1} a_{q,V_2} + a_{q,V_1} v_{q,V_2}) \int_x^1 \frac{dy}{y} \left\{ \frac{2}{3} [-q(y, \mu_F^2) + \bar{q}(y, \mu_F^2)] \right. \\ &\quad \left[-\frac{3}{4} P_{qq}(z) \log \frac{\mu_F^2 z}{Q^2} + (1 + z^2) \mathcal{D}_1(z) - \frac{3}{2} \mathcal{D}_0(z) \right. \\ &\quad \left. + 2 + z - \left(\frac{9}{2} + \frac{\pi^2}{3} \right) \delta(1 - z) \right] \left. \right\}, \end{aligned} \quad (43)$$

where $z = x/y$ and the plus distributions of Eq. (17) have been used. The Altarelli–Parisi splitting functions P_{qq} and P_{qg} are defined in Eq. (16).

Choosing the dynamical scales $\mu_R = \mu_F = Q_i = \sqrt{-q_i^2}$ at each proton leg, the QCD corrections are of moderate size, i.e. at the 10–15% level as can be inferred from Fig. 14. The relative QCD corrections develop only a minor dependence on the value of $\tan\beta$. The related scale uncertainties determined by the 7-point method are shown in Figs. 15, 16. The NLO error band lies within the LO one and reduces to residual uncertainties to a level of less than 2–10%. This uncertainty needs to be added to the one of the SFA itself. The cross section of

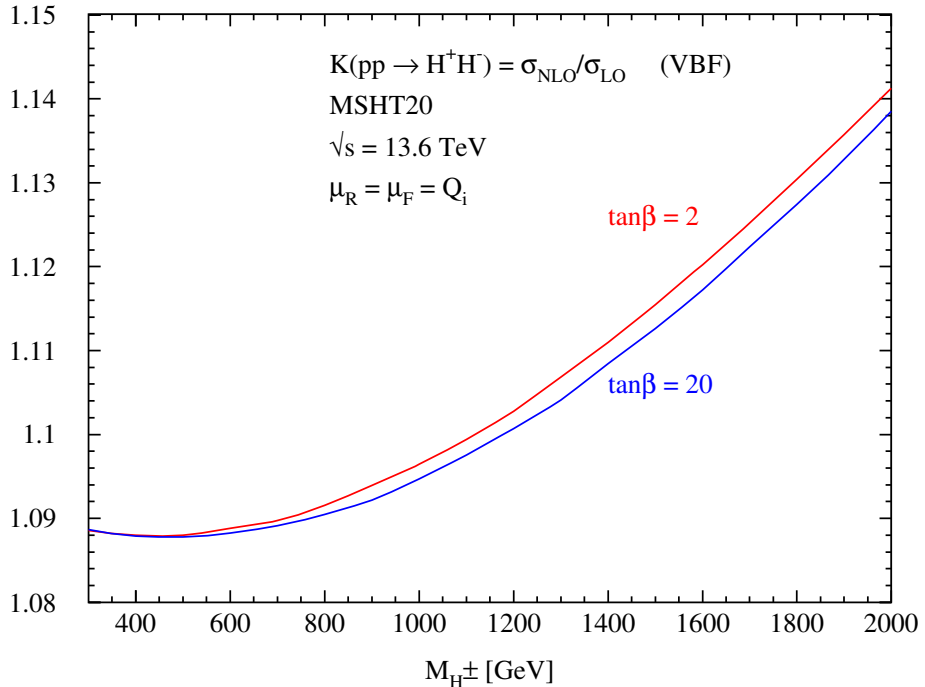


Figure 14: The K factor for the VBF cross section of charged-Higgs pair production as a function of the charged Higgs mass for the two 2HDM scenarios. The MSHT20lo_as130 and MSHT20nlo_as118 PDFs [18] were adopted for the LO and NLO cross sections, respectively.

the VBF does not develop a relevant dependence on the value of $\tan\beta$, since it is dominated by the gauge-coupling contributions.

6 Results

Using the above computations we now present and compare the different charged-Higgs pair production processes and their corresponding uncertainties. We have adopted the PDF4LHC15 NLO PDFs [19] for the determination of the PDF+ α_s uncertainties combined with the scale dependence discussed before. We have added the scale and PDF+ α_s uncertainties *linearly*, since the scale dependence does not show a significant dependence on the chosen error PDF. The results are presented in Figs. 17 and 18 for the two scenarios with $\tan\beta = 2$ and 20, respectively. The Drell–Yan-like Higgs-pair production mode dominates by one order of magnitude over the VBF and gluon-fusion processes⁷. The cross section of the Drell–Yan-like process reaches a couple of fb for smaller charged Higgs masses and drops below the ab range for charged Higgs masses above 1.5 TeV for both scenarios, while the VBF and gluon-fusion channels stay in the

⁷Charged Di-Higgs-strahlung $q\bar{q} \rightarrow H^+H^- + Z/W$ is expected to be further suppressed.

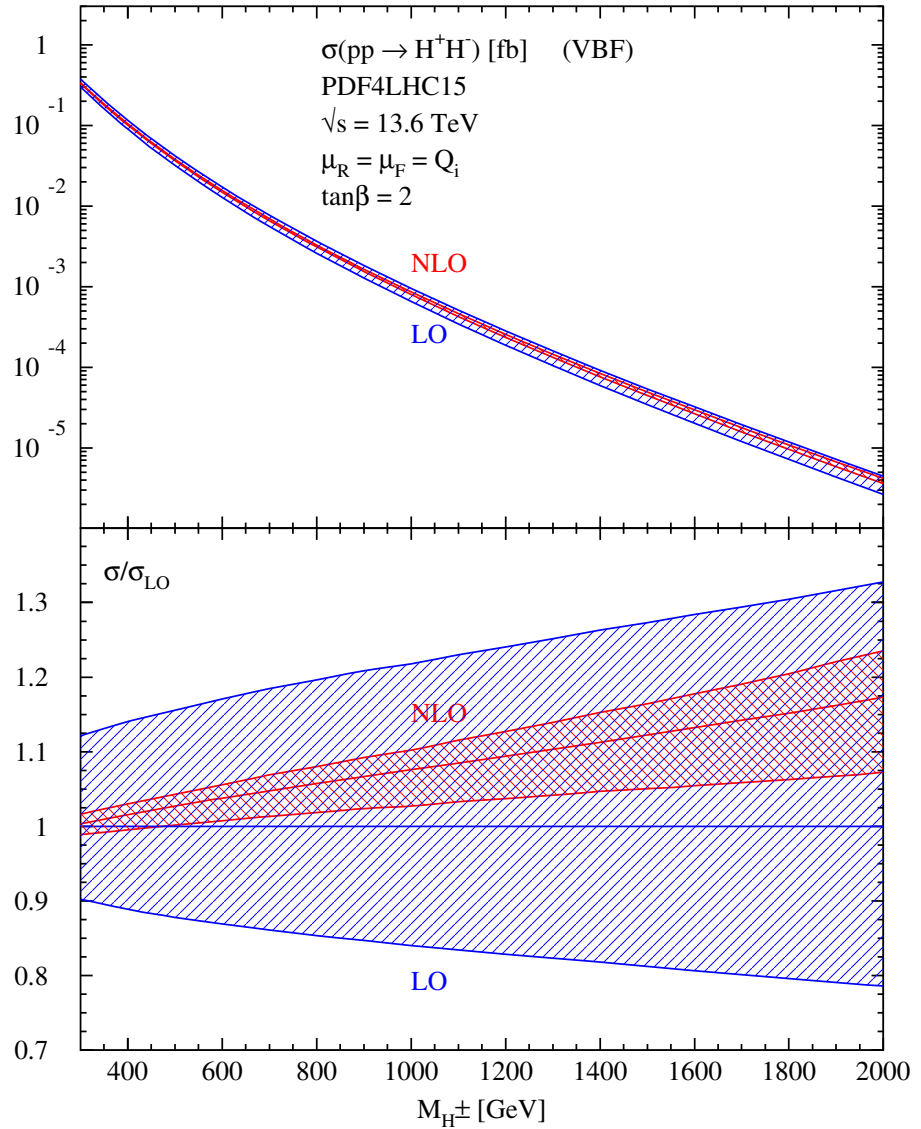


Figure 15: The cross section of VBF of charged-Higgs pair production as a function of the charged Higgs mass for $\tan\beta = 2$. The PDF4LHC15 PDFs [19] were adopted for the LO and NLO cross sections.

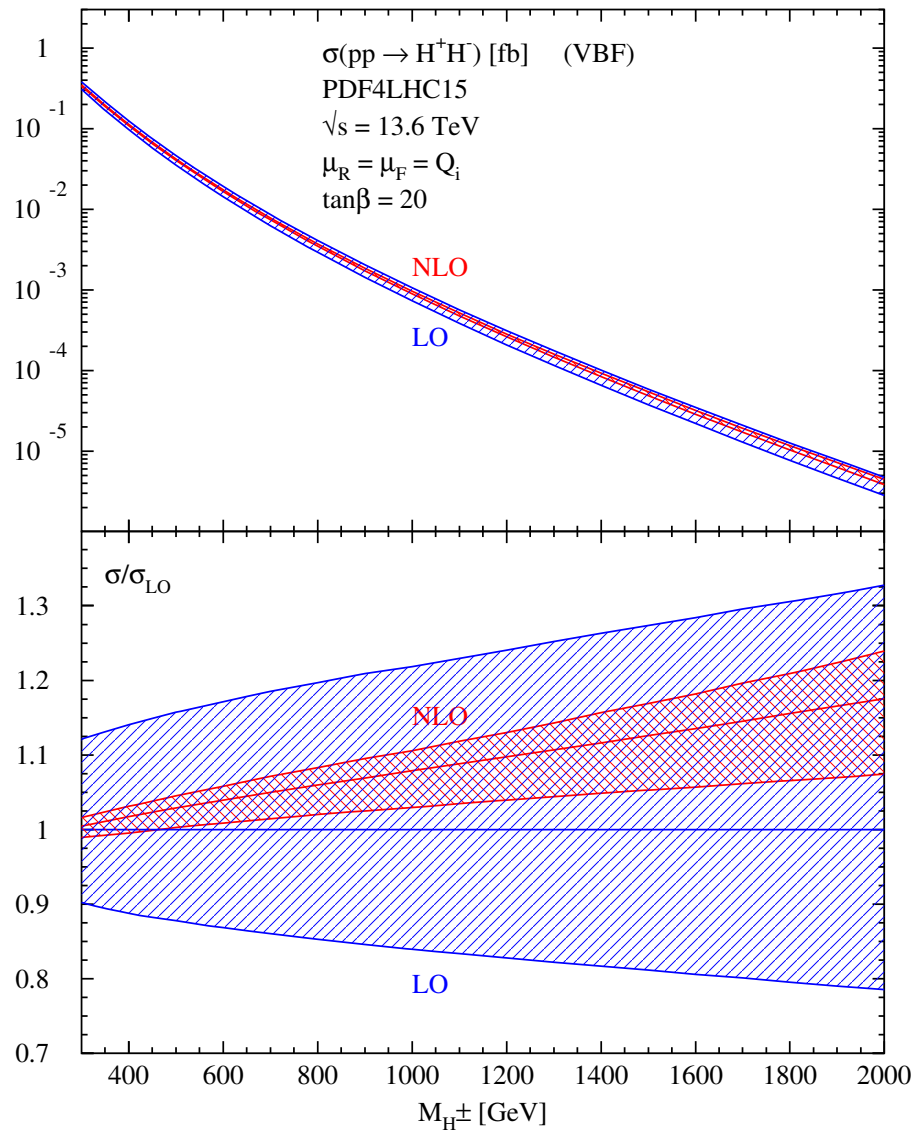


Figure 16: The same as Fig. 15 but for $\tan\beta = 20$.

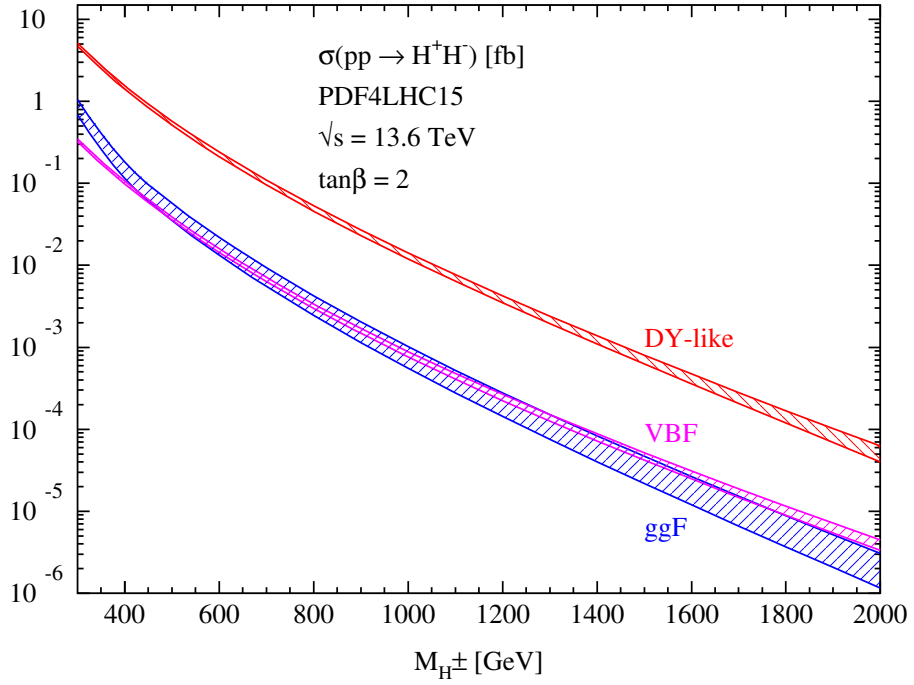


Figure 17: The total cross sections of all production modes of charged-Higgs pair production as a function of the charged Higgs mass for $\tan\beta = 2$. The PDF4LHC15 PDFs [19] were adopted for the NLO cross sections. The error bands are the sum of the scale and the PDF+ α_s uncertainties.

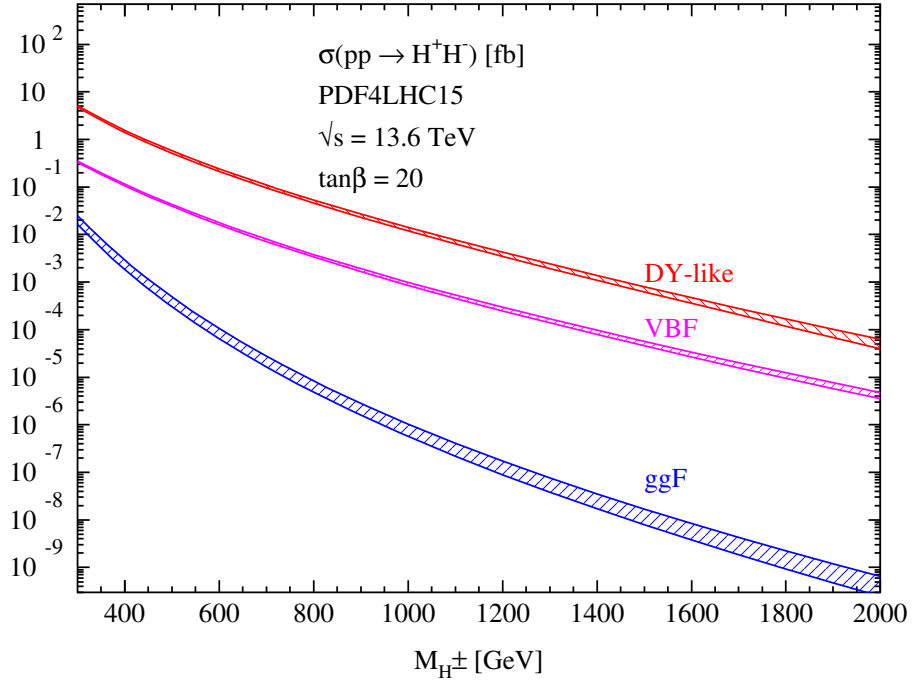


Figure 18: The same as Fig. 17 but for $\tan\beta = 20$.

sub- fb region with the VBF being the second largest production process in a significant part of the mass range.

The PDF+ α_s uncertainties of the Drell–Yan-like production mode amount to about 2–17%, thus combining with the scale uncertainties to a total theoretical uncertainty of about 4–22% depending on the charged Higgs mass. The VBF develops PDF+ α_s uncertainties of about 2–7% and combines with the scale dependence to about 3–15% total theoretical uncertainties. These are, however, modified by the uncertainties induced by the SFA. The gluon-fusion process is dominantly affected by its scale uncertainties of 20–25%, while the PDF+ α_s uncertainties amount to about 4–20% thus yielding 25–45% theoretical uncertainties in total. However, these are modified when adding the missing finite top-mass effects of about 20–30% at NLO. The gluon-fusion cross-section is suppressed for large values of $\tan\beta$ in the 2HDM of type I.

7 Conclusions

In this work we have analyzed charged Higgs-boson pair production at the LHC. These production modes of novel charged Higgs states in extended Higgs sectors exhibit direct access to some trilinear Higgs couplings and thus to parts of the BSM Higgs potential. This analysis has been performed within the 2HDM of type I. Although the cross sections for these processes are small, i.e. in the few- fb down to the below- ab range, it will be relevant to search for these charged-Higgs production modes. This work improved all contributing processes to the NLO QCD level thus allowing for a refined analysis of the associated theoretical uncertainties. The latter were determined by combining the scale uncertainties by means of the 7-point method related to the factorization and renormalization scale choices and the PDF+ α_s uncertainties emerging from the PDFs. For the final combination of the uncertainties, we adopted the NLO PDF4LHC15 PDFs and their associated error PDF sets [19], since the new PDF4LHC21 sets do not provide LO and NLO PDFs [27].

The dominant charged Higgs pair production mode is the Drell–Yan like process with photon and Z -boson exchange in the s -channel. This process is independent of the 2HDM scenario, since only gauge couplings contribute (The bottom-Yukawa induced process $b\bar{b} \rightarrow H^+H^-$ is suppressed by several orders of magnitude.). This results in residual total theoretical uncertainties of about 4–22% for the leading Drell–Yan-like mode, while the uncertainties of the subleading VBF and gluon-fusion amount to about 3–15% and 25–45%, respectively⁸. The gluon-fusion cross section is strongly suppressed for large values of $\tan\beta$ within the 2HDM of type I, thus

⁸The upper ends of the uncertainty bands emerge for large charged Higgs masses, where the PDFs contribute at large Bjorken- x values.

making VBF the second largest charged-Higgs production mode.

Acknowledgments

The authors are indebted to T. Biekötter and K. Elyaouti for helpful correspondence and to E. Vryonidou for useful discussions about Ref. [9]. We are grateful to S. Moretti for sharing his LO code for vector-boson fusion used in Ref. [10] at very early stages of this work that allowed to pin down the sources of discrepancies. The research of L.B. and Y.Y. is supported by the Swiss National Science Foundation (SNSF).

References

- [1] G. Aad *et al.* [ATLAS Collaboration], Phys. Lett. **B716** (2012) 1; S. Chatrchyan *et al.* [CMS Collaboration], Phys. Lett. **B716** (2012) 30.
- [2] P. W. Higgs, Phys. Lett. **12** (1964) 132, Phys. Rev. Lett. **13** (1964) 508 and Phys. Rev. **145** (1966) 1156; F. Englert and R. Brout, Phys. Rev. Lett. **13** (1964) 321; G. S. Guralnik, C. R. Hagen and T. W. Kibble, Phys. Rev. Lett. **13** (1964) 585; T. W. B. Kibble, Phys. Rev. **155** (1967) 1554.
- [3] G. Aad *et al.* [ATLAS and CMS Collaborations], JHEP **1608** (2016) 045; G. Aad *et al.* [ATLAS Collaboration], ATLAS-CONF-2019-005; A.M. Sirunyan *et al.* [CMS Collaboration], JHEP **01** (2021) 148.
- [4] G. 't Hooft, Nucl. Phys. B **35** (1971) 167; G. 't Hooft and M. J. G. Veltman, Nucl. Phys. B **44** (1972) 189.
- [5] T. D. Lee, Phys. Rev. D **8** (1973), 1226-1239.
- [6] G. C. Branco, P. M. Ferreira, L. Lavoura, M. N. Rebelo, M. Sher and J. P. Silva, Phys. Rept. **516** (2012), 1-102.
- [7] A. Alves and T. Plehn, Phys. Rev. D **71** (2005) 115014.
- [8] N. Kidonakis and A. Tonero, JHEP **06** (2024) 138.
- [9] B. Hespel, D. Lopez-Val and E. Vryonidou, JHEP **09** (2014), 124.
- [10] S. Moretti, J. Phys. G **28** (2002), 2567.
- [11] S. L. Glashow and S. Weinberg, Phys. Rev. D **15** (1977) 1958.

- [12] S. Kanemura, Y. Okada, E. Senaha and C. P. Yuan, Phys. Rev. D **70** (2004) 115002.
- [13] R. Coimbra, M. O. P. Sampaio and R. Santos, Eur. Phys. J. C **73** (2013) 2428; M. Mühlleitner, M. O. P. Sampaio, R. Santos and J. Wittbrodt, Eur. Phys. J. C **82** (2022) no.3, 198.
- [14] H. Bahl, T. Biekötter, S. Heinemeyer, C. Li, S. Paasch, G. Weiglein and J. Wittbrodt, Comput. Phys. Commun. **291** (2023), 108803.
- [15] E. Eichten, I. Hinchliffe, K. D. Lane and C. Quigg, Rev. Mod. Phys. **56** (1984), 579-707.
- [16] G. Altarelli, R. K. Ellis and G. Martinelli, Nucl. Phys. B **157** (1979) 461-497; J. Kubar-Andre and F. E. Paige, Phys. Rev. D **19** (1979) 221.
- [17] G. Altarelli and G. Parisi, Nucl. Phys. B **126** (1977) 298-318.
- [18] S. Bailey, T. Cridge, L. A. Harland-Lang, A. D. Martin and R. S. Thorne, Eur. Phys. J. C **81** (2021) no.4, 341.
- [19] J. Butterworth, S. Carrazza, A. Cooper-Sarkar, A. De Roeck, J. Feltesse, S. Forte, J. Gao, S. Glazov, J. Huston and Z. Kassabov, *et al.* J. Phys. G **43** (2016) 023001.
- [20] A. Krause, T. Plehn, M. Spira and P. M. Zerwas, Nucl. Phys. B **519** (1998) 85-100.
- [21] A. Djouadi, M. Spira and P. M. Zerwas, Phys. Lett. B **264** (1991), 440-446; S. Dawson, Nucl. Phys. B **359** (1991), 283-300; M. Spira, A. Djouadi, D. Graudenz and P. M. Zerwas, Nucl. Phys. B **453** (1995), 17-82.
- [22] S. Dawson, S. Dittmaier and M. Spira, Phys. Rev. D**58** (1998) 115012.
- [23] S. Borowka, N. Greiner, G. Heinrich, S. P. Jones, M. Kerner, J. Schlenk, U. Schubert and T. Zirke, Phys. Rev. Lett. **117** (2016) no.1, 012001 Erratum: [Phys. Rev. Lett. **117** (2016) no.7, 079901]; S. Borowka, N. Greiner, G. Heinrich, S. P. Jones, M. Kerner, J. Schlenk and T. Zirke, JHEP **1610** (2016) 107; J. Baglio, F. Campanario, S. Glaus, M. Mühlleitner, M. Spira and J. Streicher, Eur. Phys. J. C**79** (2019) no.6, 459; J. Baglio, F. Campanario, S. Glaus, M. Mühlleitner, J. Ronca, M. Spira and J. Streicher, JHEP **04** (2020), 181; J. Baglio, F. Campanario, S. Glaus, M. Mühlleitner, J. Ronca and M. Spira, Phys. Rev. D**103** (2021) no.5, 056002.
- [24] G. C. Cho, K. Hagiwara, J. Kanzaki, T. Plehn, D. Rainwater and T. Stelzer, Phys. Rev. D **73** (2006) 054002.

- [25] S. Gutzwiller, Diploma thesis, ETH Zurich, 2008.
- [26] M. A. Arroyo-Ureña, O. Félix-Beltrán, J. Hernández-Sánchez, C. G. Honorato and T. A. Valencia-Pérez, [arXiv:2503.03822 [hep-ph]].
- [27] T. Cridge [PDF4LHC21 combination group], SciPost Phys. Proc. **8** (2022), 101.